

Accepted Manuscript

Experimental assessment and analytical modeling of novel fiber-reinforced isolators in unbounded configuration

Daniele Losanno, Ingrid E. Madera Sierra, Mariacristina Spizzuoco, Johannio Marulanda, Peter Thomson

PII: S0263-8223(18)33877-7

DOI: <https://doi.org/10.1016/j.compstruct.2019.01.026>

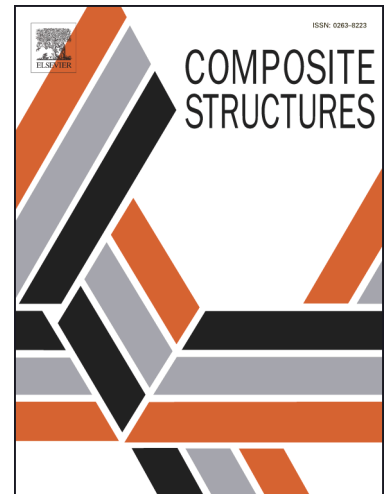
Reference: COST 10543

To appear in: *Composite Structures*

Received Date: 26 October 2018

Revised Date: 20 December 2018

Accepted Date: 2 January 2019



Please cite this article as: Losanno, D., Madera Sierra, I.E., Spizzuoco, M., Marulanda, J., Thomson, P., Experimental assessment and analytical modeling of novel fiber-reinforced isolators in unbounded configuration, *Composite Structures* (2019), doi: <https://doi.org/10.1016/j.compstruct.2019.01.026>

This is a PDF file of an unedited manuscript that has been accepted for publication. As a service to our customers we are providing this early version of the manuscript. The manuscript will undergo copyediting, typesetting, and review of the resulting proof before it is published in its final form. Please note that during the production process errors may be discovered which could affect the content, and all legal disclaimers that apply to the journal pertain.

Experimental assessment and analytical modeling of novel fiber-reinforced isolators in unbounded configuration

Daniele Losanno¹, Ingrid E. Madera Sierra^{2,3}, Mariacristina Spizzuoco¹, Johanning Marulanda³ & Peter Thomson³

¹ Department of Structures for Engineering and Architecture, University of Naples, Federico II, 21 via Claudio, Naples, Italy

² Departamento de Ingeniería Civil e Industrial, Pontificia Universidad Javeriana Cali, Calle 18 #118-200, Santiago de Cali, Colombia.

³ Escuela de Ingeniería Civil y Geomática, Universidad del Valle, Calle 13 #100-00, Santiago de Cali, Colombia.

Abstract

Base isolation system is one of the most commonly used technologies implemented around the world for seismic protection of infrastructure. Its objectives are the protection of human life and the reduction of damage to buildings as a result of earthquakes. However, the system is rarely used in developing countries such as Colombia, due to its relatively high costs, including the cost of importing the devices. The development of an isolation system using local technology therefore eliminates the latter expense. This paper focuses on the experimental assessment and analytical modeling of low-cost seismic isolators for low-rise buildings, which represent most construction projects worldwide. Two types of unbonded isolator with a high damping rubber matrix and different reinforcement fibers were employed: carbon and polyester. Scaled prototypes were manufactured and tested under compression and shear loads. Despite the lower mechanical properties of polyester, the results revealed an adequate comparison between the vertical and horizontal properties of the two isolators, with both satisfying minimum required design values. Nevertheless, when taking into account the fact that the price of polyester fiber is one order of magnitude less than of carbon, this seems to be the option with greater potential to be implemented as a low-cost seismic isolation system. Based on the experimental results, an analytical model was proposed to estimate the horizontal stiffness of unbonded isolators, taking into account the reinforcement characteristics, the effective area and the shear modulus of the rubber. In comparison with other formulations, the proposed model was found to be sufficiently accurate to be used in the preliminary design of unbonded fiber-reinforced elastomeric isolators.

Keywords: seismic isolation; fiber-reinforced isolators; unbonded isolators; horizontal stiffness; shear test; compression test.

1. Introduction

Base isolation is one of the most effective technologies in seismic protection of structures. Its objectives are the protection of human life and a reduction of the damage caused to buildings during earthquakes. Nowadays, the isolation system has been widely implemented in more than 12000 projects [1], and its effectiveness has been proved during different seismic events worldwide [2]–[4]. In view of this, the system is rarely used in emerging countries such as Colombia due to its relatively high cost. The conventional devices used in the system are steel-reinforced isolators (SREIs), which are heavy and expensive [5]. However, over the last few decades, new kinds of bearings for seismic isolation have been developed and investigated [6]–[11] in order to be lower cost. These new devices contain fiber sheets rather than steel reinforcement within the bearing and are known as fiber-reinforced elastomeric isolators (FREIs). The main difference between SREIs and FREIs is that the latter can be used without a connection to the structure, thereby reducing costs, weight, and the installation and manufacturing process times. These characteristics may lead to the implementation of the isolation system in all types of project, including residential buildings.

Reducing the cost of FREIs can be achieved by replacing the natural rubber with recycled elastomers derived from tires and industrial leftovers, scrap tire rubber pads, and nanocomposite rubber [12]–[15]. Alternatively, non-conventional materials can be used such as carbon-fiber-reinforced plastic meshes, polyamide and engineering plastic sheets [16]–[18], or low-cost fiber mesh like glass or nylon instead of carbon (bi-directional or quadri-directional fabrics) or Kevlar [5], [7], [12], [19]–[28]. In terms of behavior, the corners of unbonded FREIs (U-FREIs) roll off the supports during horizontal displacements due to the unbonded condition and the lack of flexural rigidity of the fiber reinforcement. This eliminates the high-tensile stress regions developed in a bonded isolator when it is displaced horizontally [29], [30]. As such, the shear loads at the bearing contact surfaces are transferred through friction only. For that reason, the horizontal response

characteristic of U-FREIs becomes more complex than SFREIs and their equations for horizontal stiffness evaluations are not applicable to U-FREIs [31].

In recent times, studies have been conducted to determine the mechanical characteristics of elastomeric isolators, leading to a better understanding of their performance. These investigations have been focused on determining the vertical and horizontal behavior under cyclic and monotonic loads of FREIs with different reinforcement and matrix materials, and evaluating the principal properties, such as shear modulus, damping, and vertical and horizontal stiffness. Moreover, by means of experiments and finite element analyses, the influence of geometrical parameters like the shape factor, size, height and holes has also been studied [21], [32]–[36]. As the known theory (expressions to estimate the horizontal and vertical response of isolators) is related to conventional SREIs, the results of the mentioned investigations are usually compared with the theoretical values obtained with this available information. However, in terms of the results of the experiments carried out, the lack of a complete analytical method combining the lateral and vertical response of FREIs has limited the possibility to predict their behavior, especially for strain levels up to 100%.

The research herein not only focused on the investigation of novel devices, but also on the analytical modeling of both the vertical and horizontal behavior of U-FREIs, taking into account the shear modulus and effective area variation according to the reinforcement properties. The aim of this paper is to provide a useful tool for the preliminary design of U-FREIs proposed for low-rise residential buildings, which are the most common type of project in the principal cities in Colombia. The devices were manufactured with materials and technology commercially available in the country and were to be installed in an unbonded condition, with a high damping rubber (HDR) matrix but no lead core. As the reinforcement material, a bidirectional polyester fiber mesh was proposed and compared with a carbon one. The specimens were tested under compression and shear in order to determine their mechanical properties, such as stiffness and damping. It is worth mentioning that the prototypes under investigation will also be used in bidirectional shake-table experiments to achieve a deeper understanding of their dynamic properties.

2. Analytical models for U-FREIs

Conventional SREIs are composed by rubber and thin steel plates as a form of reinforcement, with thick steel plates at the top and bottom to be connected to the structure. These isolators are relatively rigid in terms of both tension and flexion deformations. The secant horizontal stiffness is calculated with Eq. 1, where G is the shear modulus, A is the full cross-sectional area of the isolator and H_r is the total height of the rubber [37].

$$K_H = \frac{GA}{H_r} \quad (1)$$

This equation has also been used to predict the properties of U-FREIs. However, in comparison with experimental results, this solution has been found to be insufficiently accurate. The main reasons for the difference are: i) the fiber reinforcement sheets exhibit warping deformations at their ends as the bearing deforms horizontally [38]; and ii) the unbonded condition allows the top and bottom faces to roll off the contact supports when the isolator is deformed horizontally and the initial contact area is reduced for higher strain levels.

Different authors have proposed analytical models based on these features to predict the horizontal stiffness of square FREIs (Table 1). Gerhaer et al. [39], [40] considered the vertical pressure (p_z) as a modifier factor of G by suggesting Eq. 2, given an effective shear modulus (G_{eff}) (Eq. 3), where $p_{crit,0} = P_{crit}/a^2$ is the critical stress state with $P_{crit} = \sqrt{2}\pi G_{20}ASr/t_r$, $r = a/2\sqrt{3}$ [37], G_{20} the shear modulus at 20% of strain, a the length of the square isolator, d the horizontal displacement level, and r the radius of gyration. Meanwhile, Toopchi-Nezhad [38] proposed the Eq. 4, taking into account a constant value for G and the reduction of the shear area due to rollover deformation. The residual area in contact with the supports was called effective area (A_{eff}), calculated through Eq. 5, where a and b are the dimensions of the rectangular isolator, $m = 25/16\alpha H$ is the projected length of the curved part of the rollover region along the horizontal plan, with H being the total height of the isolator, which includes both the rubber and the reinforcement, and α is the geometrical parameter that relates m and the curved length, s , at a given horizontal displacement $d = s = 25/64H [2\alpha\sqrt{1 + 4\alpha^2} + \ln(2\alpha + \sqrt{1 + 4\alpha^2})]$. This means that, for a known value of d and H , α is identified and used for the calculation of A_{eff} [30].

In the same vein, Russo et al. [24] presented an expression (Eq. 6) that considers the effective area with a constant shear modulus value of the rubber at a 100% level of deformation. The effective area is calculated as the product of the isolator's side length in the direction perpendicular to the applied load, b , and the side length, a , minus the detached portion, s , in the direction parallel to the applied load (Eq. 7). The detachment starts when the level of displacement is higher than the limit value $d_0 = \sqrt{H^2 - h^2}$ (Figure 1), where H is the total initial height of the undeformed isolator and h the height of the compressed isolator (Figure 1a). Accordingly, the detached portion is calculated as $s = d - d_0$. The effective area will be the total area when the displacement level is no larger than d_0 (Figure 1b). The rollover deformation will continue until the lateral surface is all in contact with the top surface (Figure 1d) [24]. As a combination of these methods, Van Ngo et al. [31] developed an expression (Eq. 8) which includes both the variation of the shear modulus (effective shear modulus, G_{eff}) and the contact area (effective plan area, A_{eff}) according to the horizontal displacement level. In this case, G_{eff} can be calculated through two methods in the displacement range from 0 to $1.50 H_r$ (9, Eq. 10). It is worth mentioning that all these methods were developed for a square isolator.

Table 1. Suggested formulations for the prediction of the horizontal stiffness of U-FREIs

Authors	Equations	Parameters
Gerhafer et al. [35, 36]	$K_H = \frac{G_{eff}A}{H_r}$ (2)	$G_{eff} = G \left[1 - \left(\frac{p_z}{p_{crit,0} \left(1 - \left(\frac{d}{a} \right)^2 \right)} \right)^2 \right] \left(1 - \frac{d}{a} \right)$ (3)
Toopchi-Nezhad [34]	$K_H = \frac{GA_{eff}}{H_r}$ (4)	$A_{eff} = b(a - m)$ (5)
Russo et al. [17]	$K_H = \frac{GA_{eff}}{H_r}$ (6)	$A_{eff} = b(a - s)$ (7)
Van Ngo et al. [27]	$K_H = \frac{G_{eff}A_{eff}}{H_r}$ (8)	$G_{eff} = G \left[1 - \left(\frac{p_z}{p_{crit,0} \left(1 - \left(\frac{d}{a} \right)^2 \right)} \right)^2 \right] \left(1 - \frac{d}{a} \right)$ (9) $\begin{cases} G_{eff} = G \left[1 - \left(\frac{p_z}{p_{crit,0} \left(1 - \left(\frac{d}{a} \right)^2 \right)} \right)^2 \right] \left(1 - \frac{d}{a} \right) & \text{for } 0 \leq d \leq 1.0H_r \\ G_{eff} = G \left[1 - \left(\frac{p_z}{p_{crit,0} \left(1 - \left(\frac{1.0H_r}{a} \right)^2 \right)} \right)^2 \right] \left(1 - \frac{1.0H_r}{a} \right) & \text{for } 1.0t_r < d \leq 1.5H_r \end{cases}$ (10)

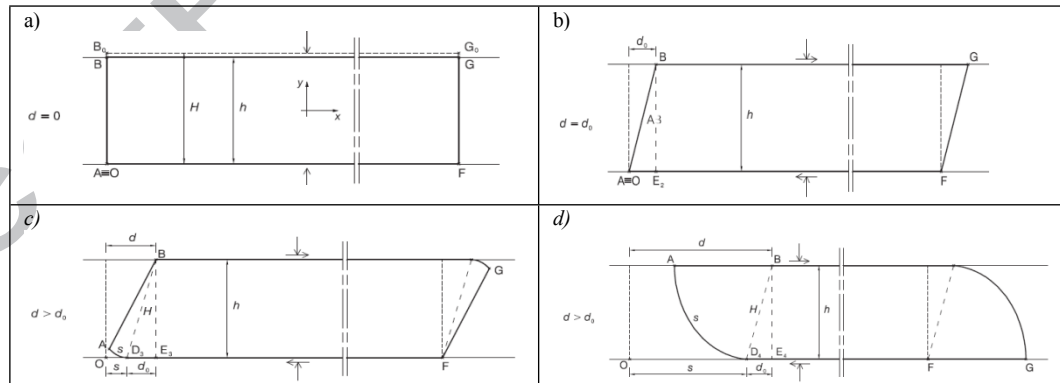


Figure 1. Deformed patterns of U-FREIs: a) under compression only, b) when the detachment starts, c) with a detached portion, and d) total rollover [24].

As a main drawback, the formulations set out in Table 1 do not explicitly take into account the influence of the type of fiber reinforcement on the horizontal stiffness and were obtained for carbon-reinforced isolators. As far as vertical behavior is concerned, Konstantinidis and Kelly [41] proposed Eq. 11 to estimate the vertical stiffness, K_V , which in turn considers the characteristics of the reinforcement material:

$$K_V = \frac{E_c^f A}{H_r} \quad (11)$$

where E_c^f is the compression modulus in the case of flexible reinforcement (i.e. fiber)[41], which is calculated using Figure 2, where $\alpha^2 = 12(1 - \nu^2)G_{20}R^2/(E_f t_f t_r)$ and $\beta^2 = 12G_{20}R^2/Kt_r^2$, with ν as the Poisson's ratio of the fiber, G_{20} is the shear modulus at a strain level of 20%, R is the radius of the isolator, E_f is the tension elastic modulus of the fiber, t_f is the thickness of the fiber reinforcement and K is the bulk modulus [42]. E_c^s is the compression modulus for the case of an isolator with rigid reinforcement (i.e. steel plates), defined as $E_c^s = 6G_{20}S^2$ for circular isolators, where the shape factor is $S = D/(4t_r)$, with D as the diameter of the device and t_r the thickness of each rubber layer.

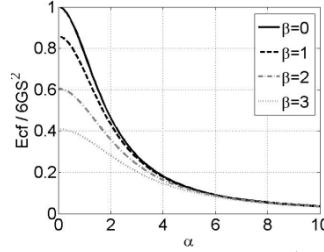


Figure 2. Dimensionless ratio of fiber-reinforced and steel-reinforced isolators' compression moduli as a function of parameter α [42].

On the basis of Eq. 2 to Eq. 11, this paper proposes a novel analytical model for a circular isolator, considering not only the shear modulus and effective area variation according to the strain level, but also the influence of the vertical flexibility under the design load.

3. Description of the isolator prototypes

The specimens used during the tests were designed for a shaking-table test campaign on a prototype building belonging to the Department of Structures for Engineering and Architecture (DiSt) at the University of Naples Federico II in Italy (Figure 3). The design process was conducted according to FEMA 450 requirements [43], considering the stiffness formulation provided for SREIs [44] and the hazard level of the site. The dimensions of the prototype were reduced by $S_L=1/3$, while $S_M=1/9$ was applied for the mass. Due to the unavailability of commercial products, and like other investigations on scaled FREIs [42], [45], [46], it is assumed that the thickness of the fiber layer cannot be scaled by S_L in a full-scale bearing. It is also worth noting that the inherent properties of the materials of the isolators (rubber, steel, fibers, etc.) were equal to those that could be used on the real structure ($S_E=1$). The structure consisted of a steel frame with two degrees of freedom, having a total height of 2900mm and plan dimensions of 2650 × 2150mm. The total mass of the structure was 77kN, with a base level of 36kN and a top level of 41kN, for a total 19kN load at the base of each column. The natural period of the real structure was assumed to be equal to 2s. According to the scale factors used, the scale for the natural period was $S_T=1/\sqrt{3}$, thus giving a natural period of the model equal to $T_D = 1.15s$. This value was used to determine the characteristics of the isolators. The set of seven ground motions was the same as that used by Calabrese et al. [42], which was compatible with the Italian Seismic Code (ISC) [47]. This selection was representative of regions in Italy with a moderate to high seismic risk, which are similar to the hazard levels in Colombia. The selected horizontal accelerograms were in compliance with the ISC for the life safety limit state of a class IV structure located in Naples (Italy) on soil type A, with a nominal life of 100 years (which corresponds to a 1900-year return period).



Figure 3. Prototype building at DiSt-University of Naples Federico II.

The maximum design displacement ($D_M = 90\text{mm}$) was calculated according to the maximum acceleration at the site under study (2.56m/s^2), for a target damping of 10%. A design shear deformation equal to $\gamma_s = 100\%$ and a vertical pressure of 4.0MPa were considered. The total horizontal stiffness (K_{HTotal}) was determined from the target period (T_D) and the total weight of the structure (W), provided by a total of four isolators:

$$K_{HTotal} = \frac{4\pi^2 W}{T_D^2 g} \quad (12)$$

According to the maximum design displacement (D_M) and the shear deformation, a total rubber height $H_r = D_M / \gamma_s = 30\text{mm}$ was calculated. The selected thickness of the rubber layer was $t_r = 2\text{mm}$, with a total number of layers $n_r = 15$. Then, the gross area (A) of the isolator was determined by Eq. 1.

Two different sets of unbonded isolators were manufactured with different flexible reinforcement and the same number of layers ($n_f = 14$): i) (P-FREI) type 1 (T1), 1.0mm bidirectional polyester fiber fabric with an elastic modulus of 1.176MPa (Figure 4a); and ii) (C-FREI) type 2 (T2), 0.23mm bidirectional carbon fiber fabric with an elastic modulus of 234.000MPa (Figure 4b). The selection of a type of reinforcement other than carbon was made from the perspective of manufacturing lower-cost isolators with even easier-to-find fibers on the local market of developing countries.

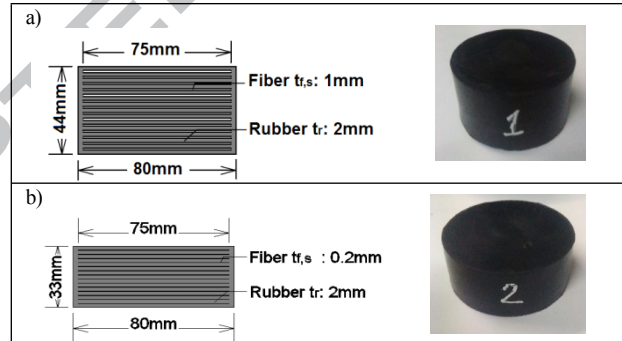


Figure 4. Cross-section of the prototypes: a) T1, and b) T2.

The manufacturing process of the isolators was divided into four steps. In the first step, the rubber and reinforcement were cut according to the required dimensions (Figure 5a). Then, each set of rubber plus fiber layers was preformed by applying vertical pressure and temperature (Figure 5b). During the third step, the complete set for each isolator was also preformed using a mold at the same temperature as in the previous step (Figure 5c). Finally, the cover part was added to the complete set and the vulcanization process was applied (Figure 5d). The union among the meshes and the rubber layers was achieved by means of an appropriate chemical adhesive, which was the same for all cases. Perforations were also made in the polyester and carbon layers to allow the rubber to fill these spaces and increase the adhesion (Figure 5a). In total, 20 specimens were tested, two for each prototype, T1 and T2, for five types of experimental tests (Table 2).

a)	b)	c)	d)
----	----	----	----

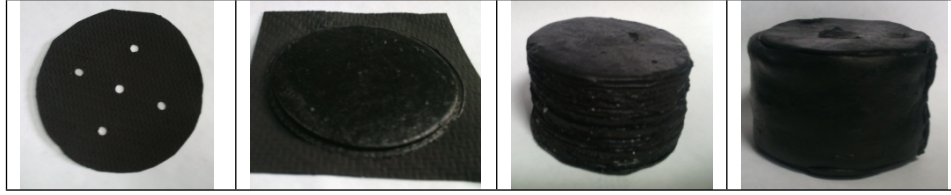


Figure 5. Manufacturing process: a) fiber layer, b) rubber and fiber layers preformed, c) complete set preformed, and d) complete set preformed and covered.

4. Experimental setups

4.1 Compression tests

Four different compression tests were performed to assess the vertical behavior of the isolators: monotonic [24], cyclic [12], maintained load [48], and ultimate load test.

Table 2. Types of isolator.

Test	Prototype	Specimen	Reinforcement	D [mm]	H [mm]	Reference
Compression - monotonic	T1	a	Polyester	78.8	43.9	T1a-1
		b		78.5	43.6	T1b-1
	T2	a	Carbon	79.5	33.4	T2a-1
		b		79.6	33.0	T2b-1
Compression - cyclic	T1	a	Polyester	78.4	43.8	T1a-2
		b		78.9	43.9	T1b-2
	T2	a	Carbon	79.3	34.3	T2a-2
		b		79.5	35.0	T2b-2
Compression - maintained	T1	a	Polyester	78.5	44.5	T1a-3
		b		78.7	43.6	T1b-3
	T2	a	Carbon	79.5	34.9	T2a-3
		b		79.5	34.1	T2b-3
Compression - ultimate	T1	a	Polyester	79.5	44.7	T1a-4
		b		79.7	45.5	T1b-4
	T2	a	Carbon	79.5	33.6	T2a-4
		b		79.4	35.1	T2b-4
Shear	T1	a	Polyester	78.8	45.0	T1a-5
		b		78.5	43.6	T1b-5
	T2	a	Carbon	79.5	32.8	T2a-5
		b		79.6	32.3	T2b-5

4.1.1 Monotonic test

Three cycles of loading–unloading were performed for each specimen, with a maximum load value that was 30% higher than the design load corresponding to 19kN (Figure 6a). The compressive load was applied quasi-statically (loading rate of 0.01mm/s) using a Humbolt HM-3000 Series Digital MasterLoader machine with a capacity of 50 kN. The displacements were measured with inductive transducers (LVDT) with ± 25 mm of stroke and 0.01 mm of precision (Figure 6b).

a)	b)
----	----

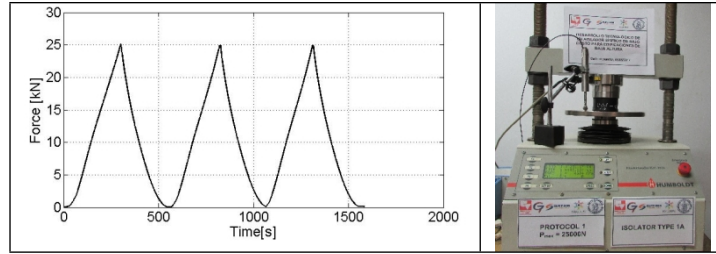


Figure 6. Monotonic compression test: a) protocol, and b) setup.

4.1.2 Cyclic test

The specimens were initially loaded monotonically (loading rate of 0.01mm/s) up to the design load ($P = 19kN$). Then, after 1min, three fully reversed triangular cycles were applied at 0.05mm/s with a $\pm 30\%$ variation with respect to the design load. After a second pause of 1min, the specimens were unloaded monotonically (loading rate of 0.01mm/s) (Figure 7a). The 1min pauses were needed to accommodate viscoelastic effects [12]. The monotonic test set up was also used during this test (Figure 7b).

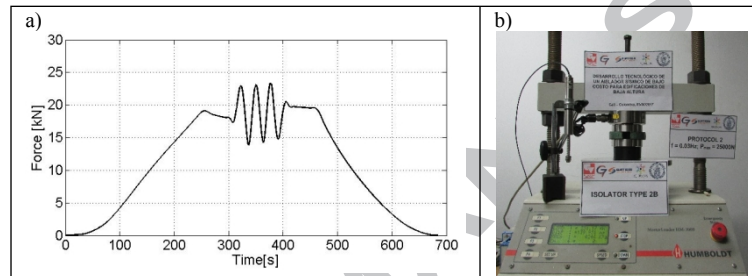


Figure 7. Cyclic compression test: a) protocol, and b) setup.

4.1.3 Maintained load test

The specimens were compressed monotonically up to a load that was 30% higher than the design load. Then, the load was kept constant for 180min (Figure 8a). Finally, the prototypes were unloaded monotonically. A WPMZD40 universal machine with a capacity of 400kN and an LVDT with ± 50 mm of stroke was used (Figure 8b).

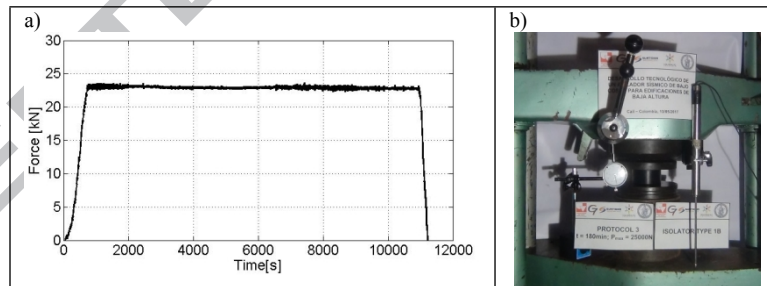


Figure 8. Maintained load: a) protocol, and b) setup

4.1.4 Ultimate load test

The prototypes were compressed until failure. The load was applied quasi-statically using the maintained load test setup (Figure 9).



Figure 9. Ultimate load test setup.

4.2 Shear test

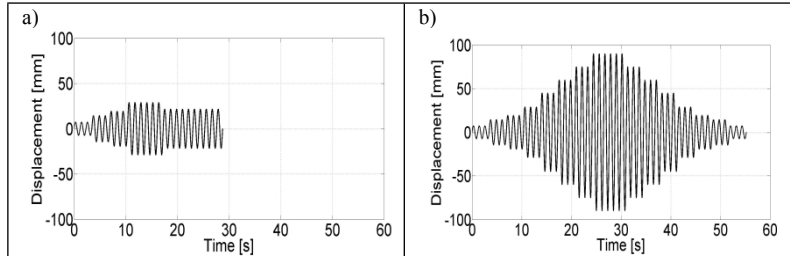
The specimens were tested under combined shear and compression loads. In order to apply the design pressure in the vertical direction, they were loaded with 19kN of force, while different displacement protocols were applied in the horizontal direction. The protocol P1 was formulated considering the FEMA 450 testing program [43], which should be carried out on isolators prior to installation using the design displacement as the maximum deformation. In order to investigate the behavior of the prototypes under larger deformations and extreme conditions, a maximum shear deformation of 300% was applied during protocol P2, i.e. a significantly higher value than the one commonly assumed for FREIs (100% - 150%) and the maximum permitted by the European Code EN 15129 [49] for SREIs (250%). Next, with the aim of evaluating the behavior dependence on the loading rate, protocol P3 was defined by increasing the period of protocol P1 under the same deformation levels. Finally, a monotonic displacement was applied during protocol P4. The characteristics of each protocol are as follows:

- P1: composed of three parts with the design period ($T_D = 1.15s$). Part 1 consisted of three fully reversed cycles of loading at each increment of displacement ($0.25D_M$, $0.50D_M$, $0.67D_M$, $1.00D_M$); in part 2, three fully reversed cycles of loading at the maximum displacement ($1.00D_M$) were applied; and in part 3, 10 continuous fully reversed cycles of loading at 0.75 times the total maximum displacement ($0.75D_M$) were used (Figure 10a) [43].
- P2: formed by the first part of P1 and four fully reversed cycles of the further displacement level ($1.50D_M$, $2.00D_M$, $2.50D_M$, $3.00D_M$). After this sequence, the devices were unloaded without a rest interval (Figure 10b). The same period as in P1 was used.
- P3: equal to P1 but with a period of 2.0s (Figure 10c).
- P4: a horizontal monotonic displacement was applied up to a 300% strain level (Figure 10d).

The relationship between the percentage of the maximum displacement, $\%D_M$, the shear deformation, γ_s , and the applied displacement, d , is presented in Table 3.

Table 3. Equivalence between the percentage of the maximum displacement, $\%D_M$, the shear deformation, γ_s , and the applied displacement, d .

$\%D_M$	γ_s [%]	Displacement (d) [mm]
0.25	25	7.2
0.50	50	14.5
0.67	67	19.4
0.75	75	21.7
1.00	100	29.0
1.50	150	43.5
2.00	200	58.0
2.50	250	72.5
3.00	300	87.0



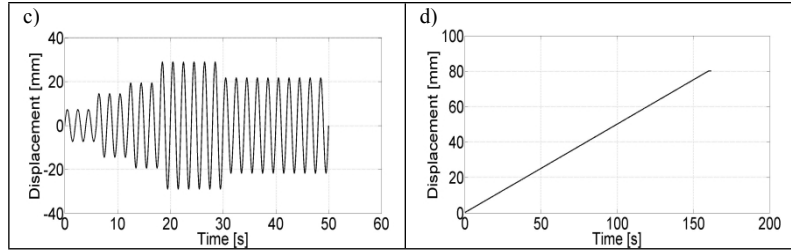


Figure 10. Displacement protocols for the shear tests: a) P1, b) P2, c) P3, and d) P4.

The shear tests were carried out at the Department of Industrial Engineering of the University of Naples Federico II - Italy. The set up for the shear tests consisted of a compression machine with a shaking table driven by a horizontal hydraulic actuator that allowed the imposition of load or displacement protocols. It was powered by a 75kW AC electric motor, with a maximum horizontal force capacity of 50kN, a maximum speed of 2.2m/s and a maximum stroke of ± 200 mm. For the tests a constant vertical load was exerted by means of a vertical hydraulic jack with a capacity of 190kN. The horizontal displacement was applied by means of recirculating ball-bearing linear guides [12]. Displacement sensors and a load cell were used to measure the sliding guides' position, the vertical load and the lateral load time-histories, respectively. A dSPACE DS1103 controller board was used for real-time control (Figure 11).

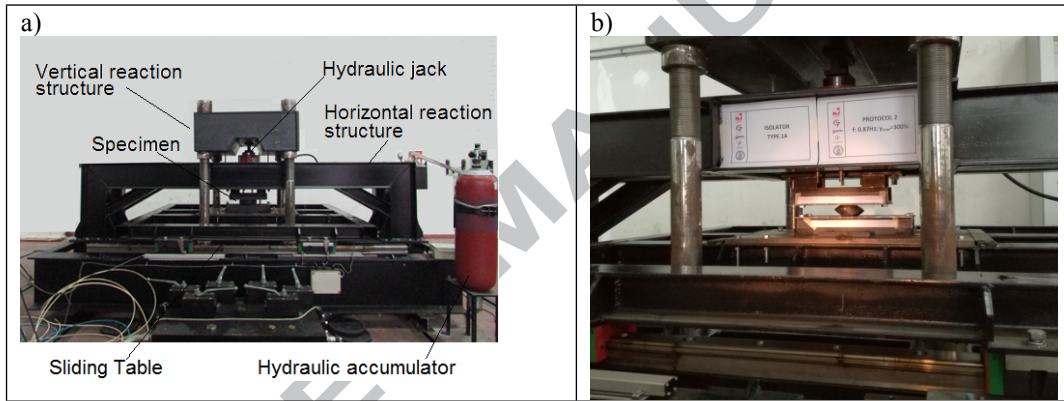


Figure 11. Shear test: a) set up, and b) specimen during the test.

5. Experimental results

5.1 Compression tests

5.1.1 Monotonic test

The force-displacement curves of Figure 12 were obtained based on the test results. The static vertical stiffness (K_{VS}) was determined by (13 [24]) (

Table 4):

$$K_{VS} = \frac{\sigma_V - \sigma_{0.3V}}{u_V - u_{0.3V}} \quad (13)$$

where u is the displacement of the specimen and σ is the stress level ($\sigma_V =$ design stress, $\sigma_{0.3V} = 0.3 \sigma_V$), defined as $\sigma = F/A$ with an applied load F and an effective area A of the specimen [50]. It is worth noting that the effective area is equal to the reinforced area without the covering part [24], and so a diameter of 75mm was used. The value obtained was compared with the theoretical vertical stiffness according to Eq. 11 and Figure 2, with α equal to 2.62 and 0.64 for polyester and carbon, respectively. In both cases, the experimental value was between 40 and 50% lower than the theoretical one (Table 4).

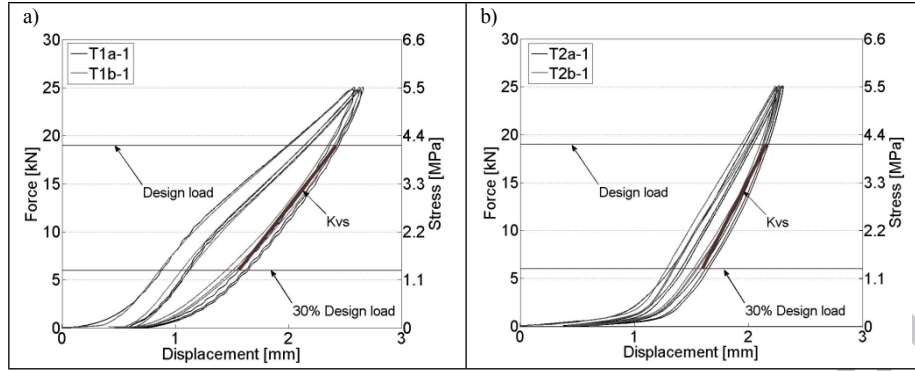


Figure 12. Force-displacement curves in monotonic compression tests: a) T1a-1, T1b-1; and b) T2a-1, T2b-1.

Table 4. Vertical stiffness – monotonic compression.

Prototype	Specimen	K_{vs} [kN/mm]				K_v [kN/mm] Theoretical	Difference [%]
		Cycle 1	Cycle 2	Cycle 3	Average		
T1	T1a-1	12	12	12	12	20	40
	T1b-1	11	12	12	12		40
T2	T2a-1	20	21	22	21	40	48
	T2b-1	20	20	20	20		50

When the prototypes were unloaded, using the final height (H_f) compared with the initial one (H_i), a residual displacement was found to be maintained in all cases (u_{res}) (Table 5), representing, in the worst case, only 1.3% of deformation (ϵ_{res}).

Table 5. Residual displacements – monotonic compression.

Prototype	Specimen	u_{res} [mm]	H_i [mm]	H_f [mm]	ϵ_{res} [%]
T1	T1a-1	0.6	43.9	43.5	1.3
	T1b-1	0.5	43.6	43.3	1.3
T2	T2a-1	0.4	33.4	32.8	1.1
	T2b-1	0.4	33.0	32.6	1.2

Based on these results, it can be inferred that this type of test could be used to obtain the static response of the isolators in terms of the maximum displacement under the design vertical load, which in this case was between 2.0 and 2.5mm in both cases.

5.1.2 Cyclic test

Figure 13 sets out the force-displacement curves obtained from the cyclic tests. The dynamic vertical stiffness (K_{vd}) was calculated using the slope of the straight lines passing through the cyclic portions of the curves [12] (Table 6). Even though the tension modulus of the carbon fiber was two orders of magnitude higher than the polyester version, the vertical stiffness of T6 was only 1.5 times lower than that of T7. This outcome can be explained by considering that vertical stiffness is related to the axial stiffness of the fiber sheet, i.e. the tension modulus multiplied by the thickness of the mesh. The combination of both parameters allowed the polyester prototypes to achieve properties similar to the carbon fiber devices, thus partially overcoming the lack of tension modulus. The maximum displacements were similar in both cases, because the rubber can be considered as unconfined (unloaded reinforcement) at the beginning of the test, due to a passive confinement against bulging, with an initial higher deformation thus occurring. After the fibers were tensioned, the isolators were laterally confined and the deformations significantly reduced.

The experimental results were compared with the theoretical ones calculated through Eq. 11 (Table 6), with a maximum difference of 5% and 27% for T6 and T7, respectively, with a better approximation in the case of polyester. These stiffness values are deemed to be representative of the expected behavior of the isolators during an earthquake, where a variation of the vertical pressure in the range $\pm 30\%$ can represent a good approximation of the load history, as the internal fibers are completely tensioned.

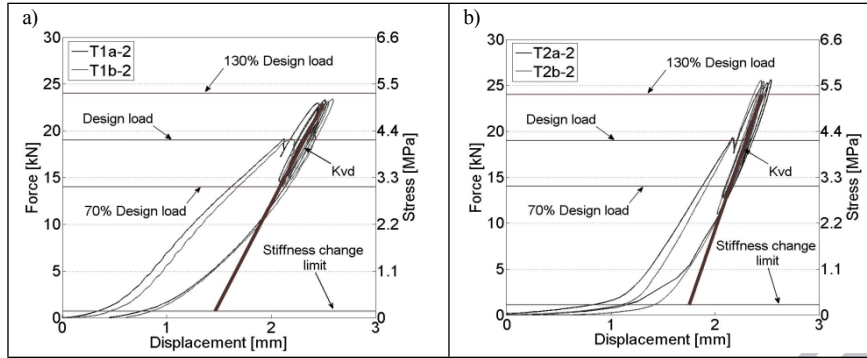


Figure 13. Force-displacement curves in cyclic compression tests: a) T1a-2, T1b-2, and b) T2a-2, T2b-2.

Table 6. Vertical stiffness – cyclic compression.

Prototype	Specimen	K_{vd} [kN/mm]				K_v [kN/mm] Theoretical	Difference [%]
		Cycle 1	Cycle 2	Cycle 3	Average		
T1	T1a-2	17	20	20	19	20	5
	T1b-2	20	20	20	20		0
T2	T2a-2	28	29	29	29	40	27
	T2b-2	31	32	31	31		22

Finally, the average vertical stiffness ($K_{vd,av}$) and average horizontal stiffness (K_H) ratio was calculated for the prototypes in each case. The average horizontal stiffness was obtained from the shear test results at the design displacement level (D_M), as explained later. Likewise, the vertical frequency and period were obtained from (14) (Table 7). The stiffness ratios were in the order of 300-400 for both isolators, showing that these values were satisfactory for providing a stable behavior of the isolators and the decoupling of the rocking motion.

$$f_v = \frac{1}{2\pi} \sqrt{\frac{K_{vd}g}{P}} \quad (14)$$

Table 7. Average vertical and horizontal stiffness ratio, vertical frequency and vertical period – cyclic compression.

Prototype	$K_{vd,av}$ [kN/mm]	K_H [kN/mm]	$K_{vd,av}/K_H$	f_v [Hz]	T_v [s]
T1	20	0.07	286	16	0.06
T2	30	0.08	375	20	0.05

5.1.3 Maintained load test

The maintained load tests results are shown in Figure 14. The T1 displacement stabilization was achieved after 30min, while T2 required only 13min. It is worth mentioning that a preload was applied to the specimens to activate the acquisition system.

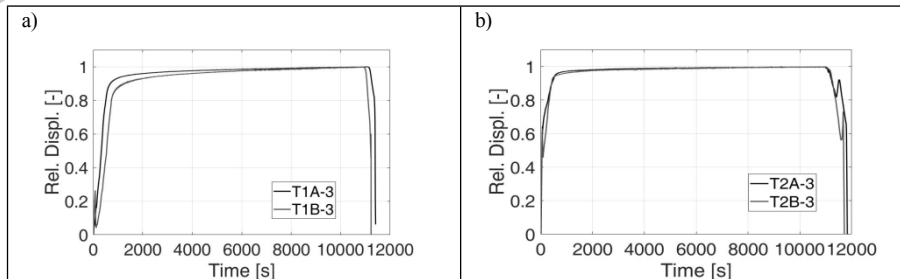


Figure 14. Force-displacement curves in maintained compression tests: a) T1A-3, T1B-3, and b) T2A-3, T2B-3.

Also, in this case, when the height before (H_i) and after (H_f) the test were compared, the deformations were almost completely recovered (Table 8).

Table 8. Height comparison of the specimens before and after the maintained compression test.

Prototype	Specimen	H_i [mm]	H_f [mm]	ϵ_{res} [%]
T1	T1a-3	44.5	44.1	0.4
	T1b-3	43.6	43.4	0.2
T2	T2a-3	34.9	33.9	1.0
	T2b-3	34.1	32.9	1.2

5.1.4 Ultimate load test

The failure of the isolators was due to the tearing at the interface between the reinforcement and the rubber layers. The phenomenon was clear in T2, where the cracking reached the top surface (Figure 15).

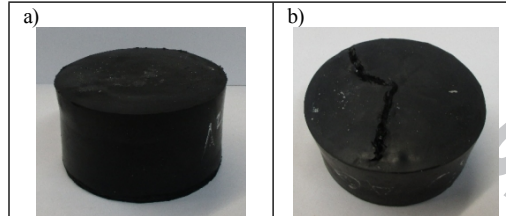


Figure 15. Failure mode in the ultimate compression tests: a) T1a-4 and b) T2a-4.

In the force-displacement curves, beyond a certain load (i.e. initial point of failure) a saw-tooth trend providing the isolators with a progressive failure mode can be observed. This involved different levels (Figure 16) redistributing the load up to a maximum. The T1 initial point of failure (P_{uo}) was around 40% higher than that for T2 (Table 9). This difference may be due to the greater flexibility of the polyester sheets, reaching the ultimate load at a higher deformation. In comparison with the design load, the initial failure point was at least 2.2 times higher (Table 9).

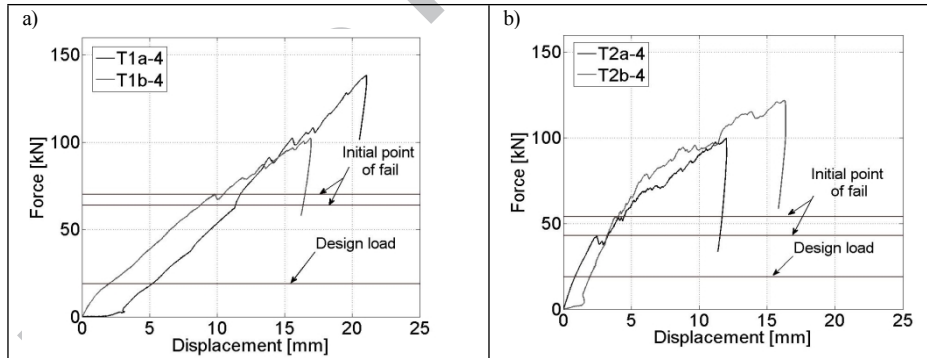


Figure 16. Force-displacement curves in the ultimate load compression tests: a) T1a-4, T1b-4 and b) T2a-4, T2b-4.

Table 9. Ultimate load compression tests results.

Prototype	Specimen	P_{uo} [kN]	P_{uo}/P
T1	T1a-4	64	3.3
	T1b-4	70	3.6
T2	T2a-4	43	2.2
	T2b-4	54	2.8

The tests were stopped before the complete failure for the T1 prototypes, due to the unstable condition of the specimens under the machine. It is worth noting that P_{uo} took place before the critical load, P_{crit} [51], was achieved for T1 and T2 (i.e. 56kN for polyester and 82kN for carbon). However, all the prototypes showed a stable behavior between P_{uo} and the end of the test.

5.2 Shear test

The static (Figure 17) and hysteretic behaviors were estimated from the shear test (Figure 18). In all cases, a stiffness reduction with respect to the first cycle was observed for each deformation level, due to the rupture of the bonds among the polymer chains and the reinforced particles (Mullins effect) [52]. The monotonic test provided a very similar response between all prototypes, with overall stable behavior up to a 300% deformation level. Figure 18 shows that the skeleton curves are enveloping the hysteresis curves obtained from protocols 2 and 3, reflecting the stable properties of the prototypes.

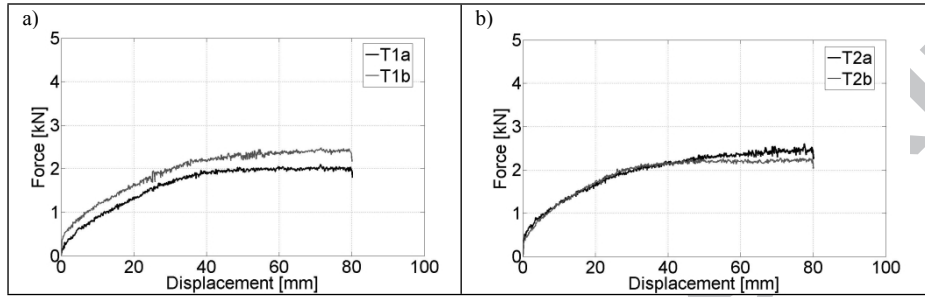
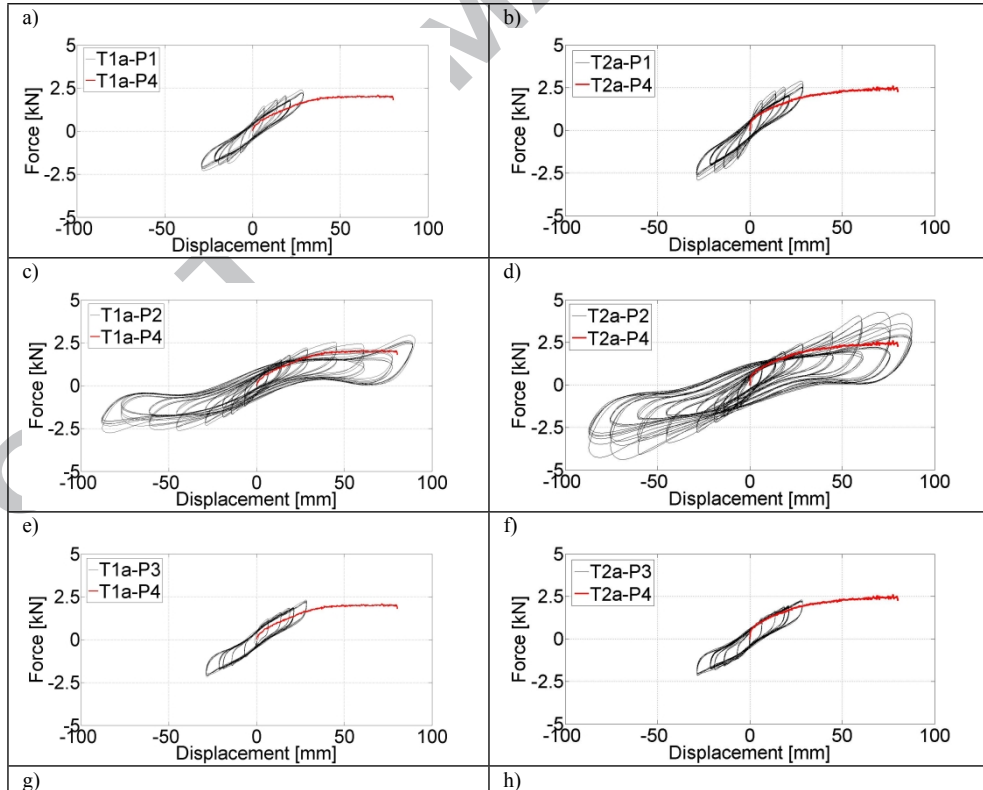


Figure 17. Force vs displacement curve for protocol P4: a) T1a and T1b, and b) T2a and T2b.

In all cases, the stiffness decreased after P1 and then the isolators achieved a stable behavior (Figure 19). This stress softening is related to the Mullins effect on filled rubber, as mentioned previously [53]. The resulting stiffness of T1 and T2 at low deformation levels is very similar, since both have the same area, rubber and connection condition. At higher deformation levels ($\epsilon > 100\%$), T2 tends to be stiffer than T1 due to the greater slenderness (total height/diameter) of the latter, with the consequence being a more significant influence of flexural deformation.



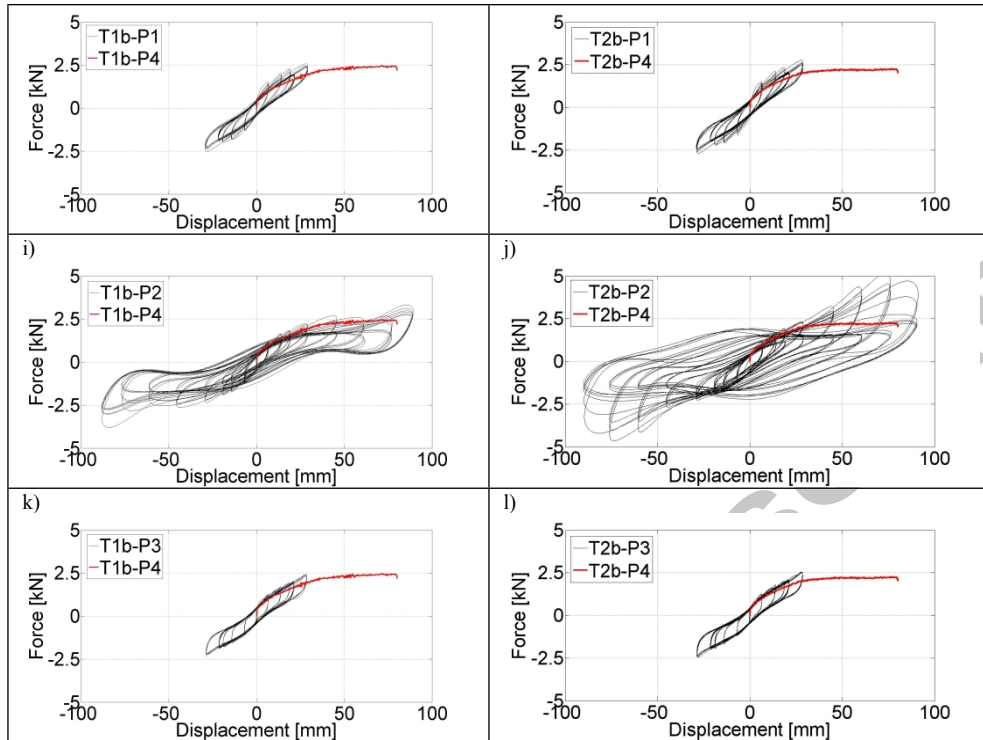


Figure 18. Force vs displacement curves in shear tests: a) T1a P1-4, b) T2a P1-4, c) T1a P2-4, d) T2a P2-4, e) T1a P3-4, f) T2a P3-4, g) T1b P1-4, h) T2b P1-4, i) T1b P2-4, j) T2b P2-4, k) T1b P3-4, and l) T2b P3-4.

As far as the influence of the vertical stiffness is concerned, even if T2 is stiffer than T1, this effect is negligible in the horizontal direction, because the maximum vertical displacement at the design load of both prototypes is similar (2.6mm and 2.3mm for T1 and T2, respectively). This phenomenon is due to the confinement effect that is triggered at a higher axial deformation level for carbon than for polyester.

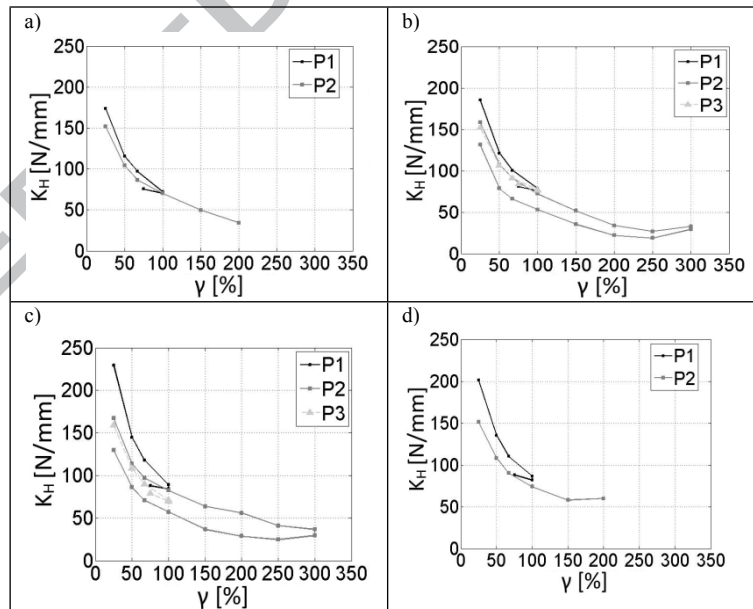


Figure 19. Horizontal stiffness (K_H) versus shear deformation (γ_s): a) T1a, b) T1b, c) T2a, and d) T2b.

It is important to highlight that all the prototypes achieved the design displacement without damage and remained undamaged after the end of P1. Damage was only observed under the loading phase of P2, after 200% strain, in prototypes T1a and T2b. For this reason, damping and stiffness values were only considered before the occurrence of this phenomenon (Table 11). Specifically, in the T1a case, tearing of the cover part of

the rubber occurred (Figure 20a), while failure occurred in PT2b due to the delamination of the carbon and rubber layers (Figure 20b). This permanent sliding at the rubber-fiber interface may be produced by a lack of adhesive impregnation during the manufacturing process. In any case, failure took place at a displacement level greater than the design value.

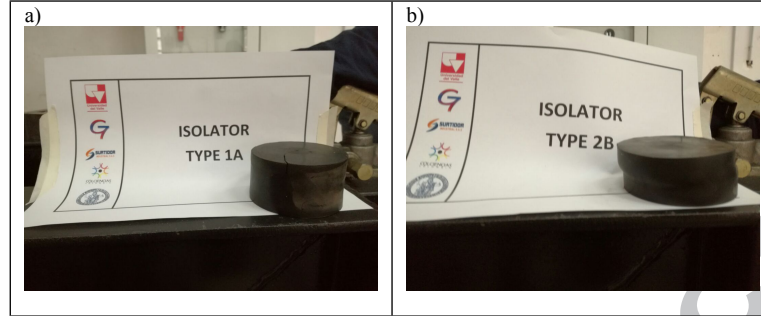
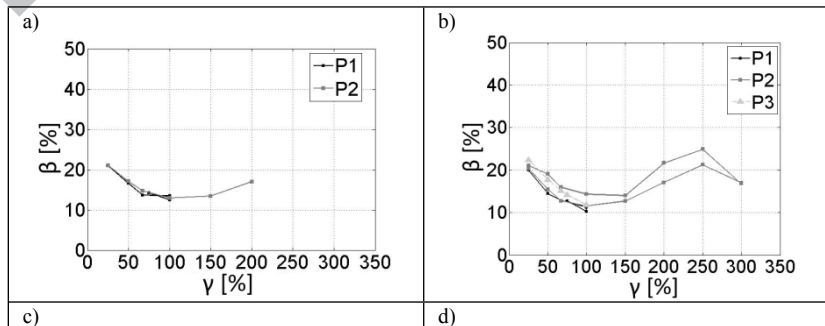


Figure 20. Failure modes of the prototypes in shear tests: a) T1a, and b) T2b.

The prototypes showed a stable rollover, in part due to the value of the second shape factor L , which is defined as the ratio between the diameter and the total rubber thickness ($L = 2.5$). The flexibility of the reinforcement allowed the unbonded surfaces to roll off until the vertical faces touched the horizontal plates. After the original vertical surfaces made contact with the horizontal supports at high deformations levels (more than 200%), the prototypes showed a positive tangent stiffness and hardening behavior (Figure 18). This hardening may be regarded as an advantage when it comes to limiting the lateral displacement under the maximum considered earthquake (MCE) [54], [55]. It is important to clarify that, due to the aforementioned failure mechanism, a negative tangent stiffness was obtained for T1a and T2b before complete rollover (Figure 18c, j).

As expected, in all cases, the equivalent damping ratio [44] was higher than the one obtained for the pure rubber (5%) [7], due to the interaction with the reinforcement. Specifically, damping ratios higher than 10% were always attained, which are expected values for SREIs with high damping rubber [7], [24]–[26], [46]. According to a previous experimental campaign conducted on the pure rubber [56], the P1 and P3 results confirmed that the properties of the isolators do not significantly depend on the load period in the examined range. Even if a viscoelastic material is expected to exhibit a frequency dependent behaviour, the high damping compound tested under shear stress in the range of period [1.25-30]s provided mechanical properties having a 8% difference with respect to minimum values. This outcome is in compliance with the code [EN 15129] [49], [49], requiring to measure stiffness and damping properties at 0.1, 0.5 and 2.0 Hz and that values at the highest and lowest frequencies shall not differ by more than 20% from the value at the middle frequency. Also, inside the range specified by FEMA450 (from 0.1 to 2 times the frequency corresponding to T_D) [43], the properties did not differ more than 15%, proving the independent behavior of the rubber to the rate of loading. Table 11 summarizes the results for the principal deformation levels of P2 during the loading phase.



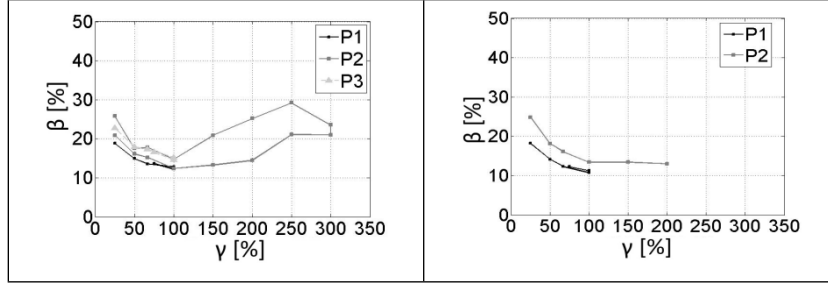


Figure 21. Damping isolators: a) T1a, b) T1b, c) T2a, and d) T1b.

Toopchi-Nezhad et al. [46] suggested, for preliminary design of a square FREI bearing, plane dimension to be larger than 2.5 times its height in order to obtain a stable rollover. In [45] and [57] the same authors show a stable rollover behavior for a bearing with an aspect ratio (side length/total height) equal to 2.8. In the proposed paper, the aspect ratio ranged from 1.7 for P-FREI to 2.3 for C-FREI with $\Lambda = 2.5$ in both cases. Even if these parameters would be lightly lower than those addressed in the different works of Toopchi-Nezhad et al., a stable behaviour was probably achieved thanks to two main features. First, the influence of the different geometry since in a circular bearing the effective area under a given lateral displacement is expected to be larger than in a square one having the same total area. Second, according to Russo and Pauletta [58], the influence of an axial load sufficiently lower than buckling one can provide a beneficial effect on the stability of FREI. In [58], the authors demonstrated that for a square isolator with an aspect ratio of 4.6, stable rollover is only achieved for an axial stress larger than 0.5 mPa, demonstrating the latter parameter playing an important role also on lateral effective stiffness. In general, a satisfactory behavior was obtained for both prototypes, demonstrating the feasibility of polyester as internal reinforcement compared to carbon fiber. Further investigations are ongoing to i) improve the manufacturing process in terms of the adhesion at the layers' interface, and ii) study the overall stability of the isolators in the case of significant rollover deformation and higher axial load.

6. Proposed analytical model

On the basis of the available formulations suggested by different authors in previous works, a more accurate analytical model is proposed here for the estimation of the horizontal stiffness of the U-FREIs. The method proposes an expression for the horizontal stiffness $K_H = G_{eff}A_{eff}/t_r$ with an effective shear modulus and contact area. The latter was evaluated taking into account the influence of the vertical behavior. This is a main difference to the work of Van Ngo et al. [31]. The model can be deemed suitable for stable isolators, i.e. with a safety factor against ultimate load larger than 2. The method can be divided into four steps:

Step 1: In the first step, the effective shear modulus (G_{eff}) is obtained from the rubber characterization curve for the expected deformation levels. This curve is usually supplied by the manufacturing company.

Step 2: In the second step, the height of the compressed isolator (h), defined as $h = H - u_p$, is estimated analytically once a compression test on a prototype isolator has been performed. This is different from other formulations [24] where this value is obtained experimentally as shown in the following example. The authors derived an expression that considers the vertical displacement under the design load (u_p) as the summation of the displacement of the unconfined (u_r) and confined rubber (u_{rf}) ((15):

$$u_p = u_r + u_{rf} \quad (15)$$

The first part, u_r , is calculated as the product of the initial height H and the deformation ε at the stiffness change limit point ($u_r = H\varepsilon$). This deformation ε is obtained from the compression test results carried out on the pure rubber once the stiffness change limit point is known from the isolator under study. The second part, u_{rf} , is calculated using the expression $u_{rf} = \Delta P/K_V$, where ΔP is the maximum applied load (P) minus the load in the stiffness change limit (P_{sc}). The theoretical vertical stiffness K_V is obtained from Eq. 11. Further investigations will be devoted to studying the stiffness change point depending on the reinforcement type.

Step 3: The effective area is calculated according to the strain level. For this purpose, the Russo et al. method was modified for a circular isolator. As a result, the isolator's portion in contact with the support and subjected to pure shear (A_{eff}) will be equal to the total area (A) minus the area of the detached semicircle (A_d) (Figure 22). The detached area is calculated as $A_d = R^2/2 * (\theta - \sin\theta)$, with $\theta = 2\arcsin(c/2R)$ and the length $c = \sqrt{((R - s/2) * 8s)}$. The detachment point (d_0) and the detached portion length (s) are calculated as $d_0 = \sqrt{H^2 - h^2}$ and $s = d - d_0$, respectively. A_{eff} is calculated as in Eq. 16 based on d_0 and the displacement level (d):

$$\begin{cases} A_{eff} = A & \text{for } d \leq d_0, \\ A_{eff} = A - A_d & \text{for } d > d_0 \end{cases} \quad (16)$$

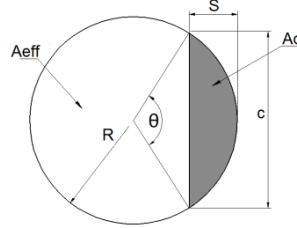


Figure 22. Effective area for circular isolators (A_{eff}).

Step 4: In the final step, K_H is calculated at different levels with the obtained values of G_{eff} and A_{eff} . Two important aspects of this method should be highlighted. First, according to Figure 1d, it is possible to assume that all the lateral surface will be in contact with the top support when $s = s_{max} = \pi H/2$. This means that the total rollover displacement is $d_{max} = d_0 + s_{max}$. The method could be applied until that point with good accuracy, i.e. until the rollover is completed. Based on the proposed equations, it can be stated that isolators experiencing higher vertical displacement under the design load P are expected to be stiffer in the horizontal direction, because the detachment process will take longer to start, thus ensuring a full contact area.

This process has been applied to the prototypes under study, as shown in the following:

Step 1: The values of G_{eff} were obtained from a shear test carried out on the pure rubber in a previous experiment conducted by the authors [56] (Figure 23).

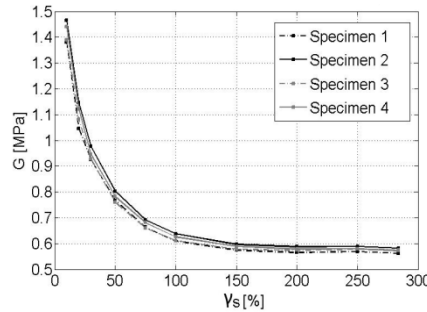


Figure 23. Shear modulus of the rubber [56].

Step 2: The deformation ε at the stress level applied to the prototypes at the stiffness change limit point was obtained from Figure 24. According to the compression cyclic test results, in the case of the polyester prototypes, the load in the stiffness change limit (P_{sc}) was 0.7kN (3.6% of the maximum load) for stress equal to 0.16MPa; in the carbon prototypes, P_{sc} was 1.1kN (5.7% of the maximum load), with stress of 0.25MPa (Figure 13). The corresponding deformation values were 3.5% and 5.5%, respectively (Figure 24). The resulting u_r are presented in Table 10. According to this comment, it comes out that the carbon fiber reinforcement is tensioned later than polyester one due to a different interaction with the rubber, and the corresponding u_r is slightly higher.

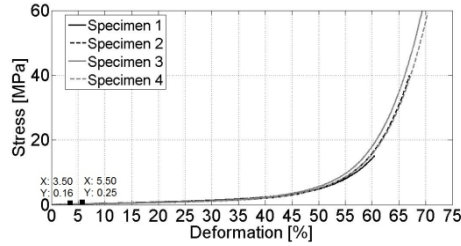


Figure 24. Stress vs deformation curves of the pure rubber under compression.

The second part, u_{rf} , was calculated using the load increment ΔP and the theoretical K_{Vd} presented in Table 6. The theoretical and experimental results are presented in Table 10 based on the analytical model. A maximum difference, $\Delta = (u_{ex} - u_p)/u_{ex}$, of 7.7 % in the worst case was deemed satisfactory for the prediction of the vertical settlement under the design vertical load. Despite a higher value of K_{Vd} , it transpired that the ratio u_r/u_{rf} was more significant in the C-FREIs, while the maximum vertical displacement at the design load of both prototypes was similar for that reason. The theoretical height of the compressed isolator, h_{th} , was calculated for a given u_{th} . It should be noted that this value is about 30% higher for the P-FREIs than the C-FREIs, thus determining a greater slenderness of the former even if the same shape factor is maintained.

Table 10. Theoretical and experimental vertical displacement comparison.

Prototype	Specimen	1 st Part			2 nd Part									
		H [mm]	ε [%]	u_r [mm]	P [kN]	P_{ec} [kN]	ΔP [kN]	K_{Vd} [kN/mm]	u_{rf} [mm]	u_p [mm]	u_{ex} [mm]	D [%]	u_r/u_{rf}	h_{th} [mm]
T1	T1a	45.0	3.5	1.6	19.0	0.7	18.3	20.0	0.9	2.5	2.6	3.8	1.8	42.5
	T1b	43.6		1.5						2.4	2.6	7.7	1.7	41.2
T2	T2a	32.8	5.5	1.8	19.0	1.1	17.9	40.0	0.4	2.2	2.3	4.3	4.5	30.6
	T2b	32.3		1.8						2.2	2.3	4.3	4.5	30.1

Step 3: The average of the theoretical detachment points, d_0 , was 14.5mm (48%) and 11.8mm (39%) for T1 and T2, respectively. The total rollover displacement values d_{max} were 83mm and 63mm for T1 and T2, corresponding to 276% and 210%, respectively. The A_{eff} for each displacement level was calculated based on these results and is presented in Figure 25, which includes the results obtained with the formulations proposed by Toopchi-Nezhad et al. [38], Russo et al. [24] and Van Ngo et al. [31].

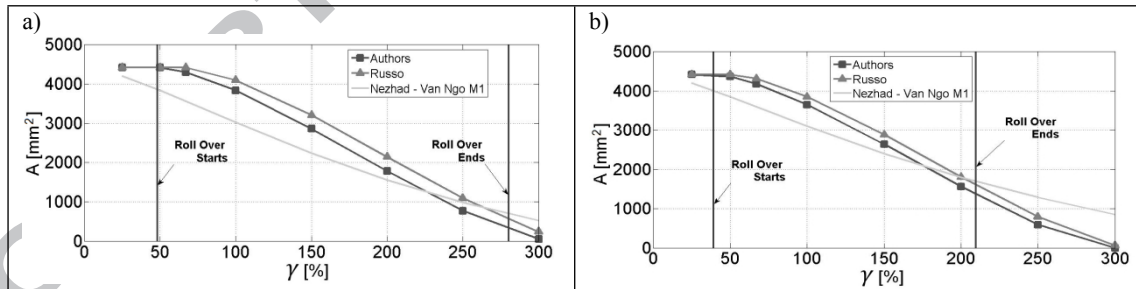


Figure 25. Theoretical effective area from different authors: a) T1, and b) T2.

Step 4: K_H was calculated taking into account the results of the previous steps. From a comparison of the theoretical K_H with the experimental version (Figure 26, Table 11), very good agreement was observed up to 250% (T1) and 150% (T2) of strain, which was close to levels where the rollover was completed according to the theoretical provisions (276% for T1 and 210% for T2). There was a percentage of difference lower than 20% in both cases. This result seems to be consistent with the behavior in the experiment, where the rollover starts immediately below 50% in both cases and reaches full contact between 200 and 250%.

Different to the prediction of the suggested method, T2 was also lightly stiffer than T1 in the horizontal direction. As the difference was less than 10%, it can be claimed that this possibly occurred due to the greater influence of the bending deformation in the horizontal response of the P-FREIs compared to the C-FREIs, with the former

being taller due to thicker fiber sheets. Future developments will include this parameter in the proposed methodology to better predict the horizontal behavior of U-FREIs with a slender geometry. In the case of higher values of the secondary shape factor, the method provides better results, as shown in the following for different experimental findings.

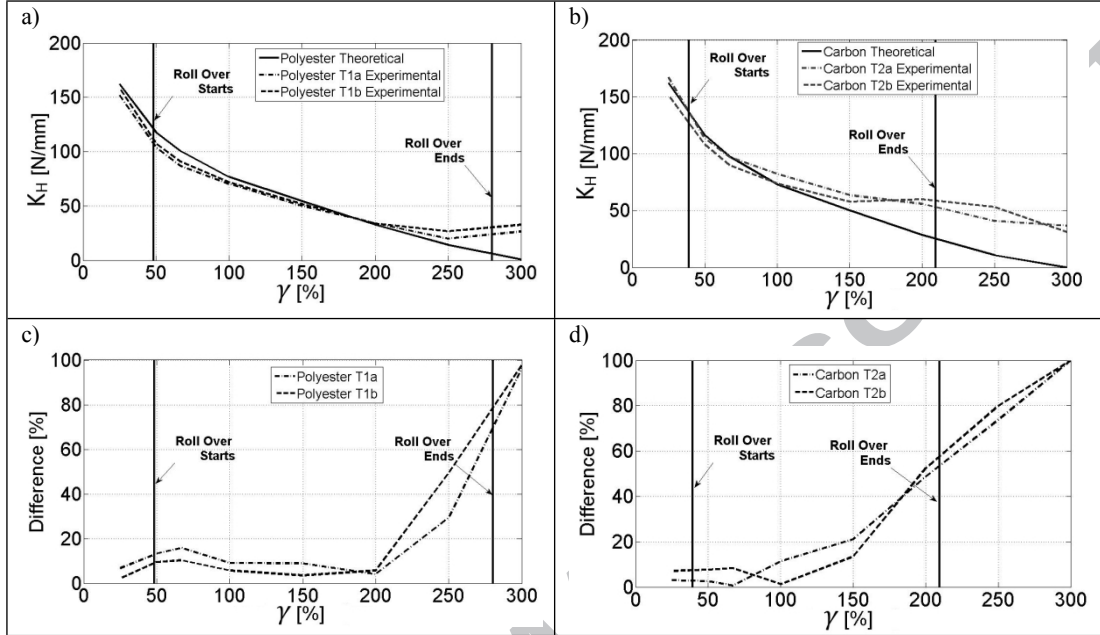


Figure 26. Theoretical and experimental comparison of the horizontal stiffness: a) T1, b) T2, c) percentage of difference T1, and d) percentage of difference T2.

Table 11. Theoretical and experimental horizontal stiffness comparison and the damping ratio for $\gamma_s = 25\%$, 50% , 100% , 150% and 200% .

Prototype	Specimen	$\gamma_s=25\%$				$\gamma_s=50\%$				$\gamma_s=100\%$			
		K_{Hth} [N/mm]	K_{Hex} [N/mm]	%Diff	β [%]	K_{Hth} [N/mm]	K_{Hex} [N/mm]	%Diff	β [%]	K_{Hth} [N/mm]	K_{Hex} [N/mm]	%Diff	β [%]
1	a	161.9	151.7	6.8	21.0	117.8	104.0	13.3	17.0	76.7	70.3	9.1	12.9
	b	161.9	158.5	2.2	20.3	117.8	107.5	9.6	15.4	76.0	72.0	5.7	11.6
2	a	161.9	167.1	3.1	20.9	116.7	113.5	2.8	16.1	73.4	82.4	10.9	12.4
	b	161.9	151.3	7.1	24.8	116.6	108.1	7.8	18.2	73.3	73.9	0.8	13.4

Prototype	Specimen	$\gamma_s=150\%$				$\gamma_s=200\%$			
		K_{Hth} [N/mm]	K_{Hex} [N/mm]	%Diff	β [%]	K_{Hth} [N/mm]	K_{Hex} [N/mm]	%Diff	β [%]
1	a	54.4	49.9	8.9	13.4	32.7	34.1	4.2	17.0
	b	53.7	51.8	3.6	12.7	32.0	33.9	5.7	17.1
2	a	50.6	63.6	20.5	13.3	29.0	55.9	48.1	14.5
	b	50.4	57.9	12.9	13.4	28.9	59.9	51.8	13.0

The comparison of the experimental and analytical results with respect to horizontal stiffness is shown in Figure 27, and includes the formulations displayed in Table 1. For the sake of brevity, the results for only one specimen of T1 and T2 will be detailed. With this aim, the suggested expressions were adapted to a circular isolator, while the initial shear modulus (G) used was the corresponding value at 20% of strain. The exception was the Russo et al. method, where the value at 100% of strain was adopted. The experimental area in Toopchi-Nezhad's

formulation provides the maximum difference (50% for polyester and 40% for carbon, up to 200% strain) with respect to the experimental results. This is probably because it does not contemplate the variation of the shear modulus (G) and, from the beginning, considers a portion detached from the contact surface despite the fact that rollover starts at between 40% and 50% of strain. With the Gerhafer model, the same values are obtained for both types of isolators, since it does not take into account the influence of the reinforcement properties and the area variation (A). In the Van Ngo model, the second method presents a better approximation to the experimental results for C-FREIs, due to the considered variation of both G and A according to the strain levels. Like Gerhafer, the same values are also obtained for the two prototypes in this case. The best match was obtained by the proposed method and that of Russo et al., with the latter assuming a constant value of G . It is also worth mentioning that Russo et al. evaluated vertical deformation experimentally, whereas the current method provides an analytical tool for the assessment of this parameter.

The proposed methodology was also applied to predict the horizontal stiffness of two different U-FREIs tested in a previous experiment conducted by the authors [56]: i) type A with a bidirectional nylon fiber (thickness 1mm); and ii) type B with two unidirectional carbon fiber meshes (thickness 0.1mm). Both types of isolator had an internal diameter of 130mm, 12 layers of rubber ($t_r = 2.5\text{mm}$, $H_r = 30\text{mm}$) and 11 layers of fiber, with a secondary shape factor of 4.3. The values plotted in Figure 28a and Figure 28b correspond to the results of the shear tests carried out on the specimens under a constant vertical load of 100kN, with a vertical settlement of 11mm and 7mm, respectively. As a result, very good agreement between the theoretical and experimental values was obtained, with a maximum difference of 8% and 10% for nylon and carbon, respectively, in the deformation level range between 0% and 300%. It can be stated that, during the test, rollover was not completed at 300% in both cases, whereas it started between 50 and 100%, as predicted by the method. Regarding the influence of the reinforcement, nylon FREIs, which were more flexible in the vertical direction, were also stiffer in the horizontal one, as predicted theoretically. This outcome confirms the adequacy of the procedure in cases where the second shape factor is higher.

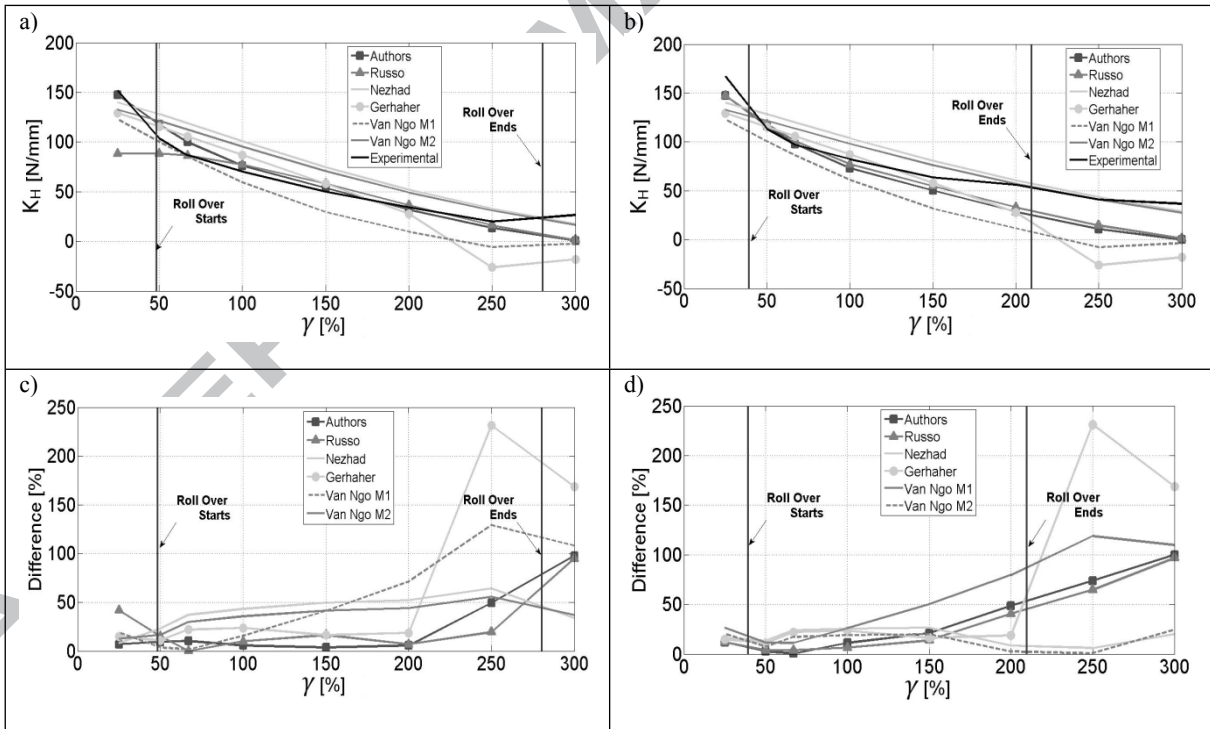


Figure 27. Theoretical approach from different authors and comparison of the horizontal stiffness experimentally: a) T1; b) T2; c) percentage of difference T1; and d) percentage of difference T2.

a)	b)
----	----

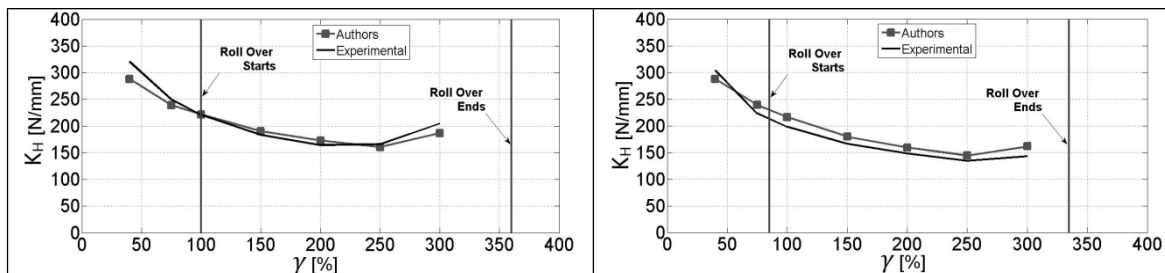


Figure 28. Theoretical approach of the authors and experimental comparison of the horizontal stiffness [52]: a) TA, and b) TB.

6. Conclusions

This paper presents a thorough investigation of novel U-FREIs reinforced with polyester fiber, which, based on the satisfactory behavior shown during experiments, could be a viable alternative to carbon-reinforced isolators. The same prototypes of P-FREIs and C-FREIs will later be adopted in a shaking-table test investigation to achieve a deeper understanding of their mechanical behavior. The results highlight an interesting comparison between the vertical and horizontal properties of P-FREIs and C-FREIs, with both satisfying required design values. Nevertheless, taking into account the fact that the price of polyester fiber is much less than carbon fiber, this seems to be a very promising option, with greater potential to be implemented as a low-cost seismic isolation system in developing countries.

A cyclic compression test is recommended to evaluate the vertical stiffness of FREIs, with a variation of the applied vertical load representing the case of an earthquake and thus simulating real conditions faced by the isolators during their service life. The satisfactory behavior of FREIs was obtained with both types of fiber in the horizontal direction. This was due to lower stress at the interface between the different layers, achieving strain levels up to 250% (which is significantly higher than the design level of 100%) without failing, and approximately 15% of equivalent damping at deformation levels higher than 100%.

On the basis of experimental results, an analytical formulation was developed to estimate the horizontal stiffness of U-FREIs, also taking into account the vertical flexibility. The analytical model proposed by the authors allows horizontal stiffness values close to the experimental ones to be obtained, with a difference of less than 20% in the range of the design deformation (up to 250% for P-FREIs and 150% for C-FREIs). The formulation was compared extensively with other authors' suggestions and its accuracy was also validated by means of additional experiments that referred to high shape factor FREIs, providing excellent results. This methodology could therefore be used to predict the horizontal behavior of FREIs with different flexible reinforcement, taking into account both the effective shear modulus and contact area considering the influence of fibers on the vertical behavior.

Further investigations will be devoted to improving the manufacturing process and conducting stability analyses under large rollover deformation, as well as to modeling the influence of critical axial load and the additional flexibility of slender and low-shape factor geometries.

7 Acknowledgements

This research was supported financially by grant FP44842-020-2017, code 1106-745-58316, from the Administrative Department of Science and Technology of Colombia COLCIENCIAS and the Universidad del Valle through Convocatoria 745-2016. The authors would like to acknowledge the scholarship for Colombian Doctoral Formation No. 617 / 2013, which was provided by COLCIENCIAS, and the collaboration of Prof. Giorgio Serino and Salvatore Strano from the Department of Structures for Engineering and Architecture at the University of Naples, Federico II.

8 References

- [1] W. Mason, "Seismic Isolation--The Gold Standard of Seismic Protection," *Struct. Mag*, 2015.
- [2] D. Gomez, J. Marulanda, and P. Thomson, "Control systems for dynamic loading protection of civil

- structures,” *Dyna-Colombia*, vol. 75, no. 155, pp. 77–89, 2008.
- [3] M. Melkumyan, “Seismic Isolation Retrofitting Experience in Armenia and New Structural Concept for an Existing 8-Story Reinforced Concrete Hospital Building to be Retrofitted by Base Isolation,” vol. 3, 2014.
- [4] D. Losanno, H. A. Hadad, and G. Serino, “Design charts for eurocode-based design of elastomeric seismic isolation systems,” *Soil Dyn. Earthq. Eng.*, no. January, pp. 1–11, 2018.
- [5] B. S. Kang, G. J. Kang, and B. Y. Moon, “Hole and lead plug effect on fiber reinforced elastomeric isolator for seismic isolation,” *J. Mater. Process. Technol.*, vol. 140, no. 1–3 SPEC., pp. 592–597, 2003.
- [6] I. E. M. S. J. M. J. . P. T., “Matrix and reinforcement materials for low-cost building isolators: an overview of results from experimental tests and numerical simulations,” *Appl. Res. Technol. J.*, vol. 16, pp. 99–111, 2018.
- [7] A. Strauss, E. Apostolidi, T. Zimmermann, U. Gerhaher, and S. Dritsos, “Experimental investigations of fiber and steel reinforced elastomeric bearings: Shear modulus and damping coefficient,” *Eng. Struct.*, vol. 75, pp. 402–413, 2014.
- [8] F. Greco, R. Luciano, G. Serino, and N. Vaiana, “A mixed explicit–implicit time integration approach for nonlinear analysis of base-isolated structures,” *Ann. Solid Struct. Mech.*, 2017.
- [9] D. Losanno, M. Spizzuoco, and G. Serino, “Optimal design of the seismic protection system for isolated bridges,” *Earthquakes Struct.*, vol. 7, no. 6, pp. 969–999, 2014.
- [10] D. Losanno, H. A. Hadad, and G. Serino, “Seismic behavior of isolated bridges with additional damping under far-field and near fault ground motion,” *Earthq. Struct.*, vol. 13, no. 2, pp. 119–130, 2017.
- [11] D. Losanno, I. E. Madera Sierra, M. Spizzuoco, J. Marulanda, and P. Thomson., “Bidirectional shake table tests results and comparison of unbounded elastomeric isolators reinforced with carbon and polyester fibers,” *Struct. Control Heal. Monit.*, vol. Under revi, 2018.
- [12] M. Spizzuoco, A. Calabrese, and G. Serino, “Innovative low-cost recycled rubber–fiber reinforced isolator: experimental tests and finite element analyses,” *Eng. Struct.*, vol. 76, pp. 99–111, 2014.
- [13] H. K. Mishra, A. Igarashi, and H. Matsushima, “Finite element analysis and experimental verification of the scrap tire rubber pad isolator,” *Bull. Earthq. Eng.*, vol. 11, no. 2, pp. 687–707, 2013.
- [14] A. Turer and B. Özden, “Seismic base isolation using low-cost Scrap Tire Pads (STP),” *Mater. Struct. Constr.*, vol. 41, no. 5, pp. 891–908, 2008.
- [15] S. Khanlari, G. D. Ashkezari, M. Kokabi, and M. R. Kashani, “Fiber-reinforced nanocomposite seismic isolators: Design and manufacturing,” *Polym. Compos.*, vol. 31, no. 2, pp. 299–306, 2010.
- [16] A. Karimzadeh Naghshineh, U. Akyüz, and A. Caner, “Comparison of fundamental properties of new types of fiber-mesh-reinforced seismic isolators with conventional isolators,” *Earthq. Eng. Struct. Dyn.*, vol. 43, no. 2, pp. 301–316, 2014.
- [17] A. Bakhshi, M. H. Jafari, and V. Valadoost Tabrizi, “Study on dynamic and mechanical characteristics of carbon fiber- and polyamide fiber-reinforced seismic isolators,” *Mater. Struct.*, vol. 47, no. 3, pp. 447–457, 2013.
- [18] P. Tan, K. Xu, B. Wang, C. M. Chang, H. Liu, and F. L. Zhou, “Development and performance evaluation of an innovative low-cost seismic isolator,” *Sci. China Technol. Sci.*, vol. 57, no. 10, pp. 2050–2061, 2014.
- [19] B. Y. Moon, G. J. Kang, B. S. Kang, and J. M. Kelly, “Design and manufacturing of fiber reinforced elastomeric isolator for seismic isolation,” *J. Mater. Process. Technol.*, vol. 130–131, pp. 145–150, 2002.
- [20] V. Venu and P. Aswathy, “Finite Element Analysis of Kevlar Reinforced Rubber as Seismic Isolator,” vol. 5, no. V, pp. 774–779, 2017.
- [21] N. C. Van Engelen, D. Konstantinidis, and M. J. Tait, “Structural and nonstructural performance of a seismically isolated building using stable unbonded fiber-reinforced elastomeric isolators,” *Earthq. Eng. Struct. Dyn.*, vol. 45, no. 3, pp. 421–439, 2016.
- [22] B. Y. Moon, G. J. Kang, B. S. Kang, G. S. Kim, and J. M. Kelly, “Mechanical properties of seismic isolation system with fiber-reinforced bearing of strip type,” *Int. Appl. Mech.*, vol. 39, no. 10, pp. 1231–1239, 2003.
- [23] G. D. Ashkezari, A. A. Aghakouchak, and M. Kokabi, “Design, manufacturing and evaluation of the performance of steel like fiber reinforced elastomeric seismic isolators,” *J. Mater. Process. Technol.*, vol. 197, no. 1–3, pp. 140–150, 2008.
- [24] G. Russo, M. Pauletta, and A. Cortesia, “A study on experimental shear behavior of fiber-reinforced elastomeric isolators with various fiber layouts, elastomers and aging conditions,” *Eng. Struct.*, vol. 52, pp. 422–433, 2013.
- [25] F. Hedayati Dezfali and M. S. Alam, “Performance of carbon fiber-reinforced elastomeric isolators manufactured in a simplified process: experimental investigations,” *Struct. Control Heal. Monit.*, vol. 21, no. 11, pp. 1347–1359, 2014.
- [26] F. Hedayati Dezfali and M. S. Alam, “Sensitivity analysis of carbon fiber-reinforced elastomeric isolators based on experimental tests and finite element simulations,” *Bull. Earthq. Eng.*, vol. 12, no. 2, pp. 1025–1043, 2014.
- [27] A. Mordini and A. Strauss, “An innovative earthquake isolation system using fibre reinforced rubber bearings,” *Eng. Struct.*, vol. 30, no. 10, pp. 2739–2751, 2008.
- [28] G. J. Kang and B. S. Kang, “Dynamic analysis of fiber-reinforced elastomeric isolation structures,” *J. Mech.*

- Sci. Technol.*, vol. 23, no. 4, pp. 1132–1141, 2009.
- [29] H. Toopchi-Nezhad, M. J. Tait, and R. G. Drysdale, “Bonded versus unbonded strip fiber reinforced elastomeric isolators: Finite element analysis,” *Compos. Struct.*, vol. 93, no. 2, pp. 850–859, 2011.
- [30] N. C. Van Engelen, P. M. Osgoeei, M. J. Tait, and D. Konstantinidis, “Partially bonded fiber-reinforced elastomeric isolators (PB-FREIs),” *Struct. Control Heal. Monit.*, vol. 22, no. 3, pp. 417–432, 2015.
- [31] S. K. an Ngo, Thuyet; Dutta, Anjan; Deb, “Evaluation of horizontal stiffness of fibre-reinforced elastomeric isolators,” *Earthq. Eng. Struct. Dyn.*, vol. 46, pp. 1747–1767, 2017.
- [32] I. Gjorgjiev and M. Garevski, “A polynomial analytical model of rubber bearings based on series of tests,” *Eng. Struct.*, vol. 56, pp. 600–609, 2013.
- [33] P. M. Osgoeei, M. J. Tait, and D. Konstantinidis, “Finite element analysis of unbonded square fiber-reinforced elastomeric isolators (FREIs) under lateral loading in different directions,” *Compos. Struct.*, vol. 113, no. 1, pp. 164–173, 2014.
- [34] P. M. Osgoeei, N. C. Van Engelen, D. Konstantinidis, and M. J. Tait, “Experimental and finite element study on the lateral response of modified rectangular fiber-reinforced elastomeric isolators (MR-FREIs),” *Eng. Struct.*, vol. 85, pp. 293–303, 2015.
- [35] Y. M. Al-Anany and M. J. Tait, “A numerical study on the compressive and rotational behavior of fiber reinforced elastomeric isolators (FREI),” *Compos. Struct.*, vol. 133, pp. 1249–1266, 2015.
- [36] G. Gioacchini, M. E. Tornello, and C. D. Frau, “Validación de un modelo numérico para un nuevo dispositivo de aislamiento sísmico,” *Asoc. Argentina Mecánica Comput.*, vol. XXXII, pp. 793–805, 2013.
- [37] J. M. Kelly and D. Konstantinidis, *Mechanics of rubber bearings for seismic and vibration isolation*. John Wiley & Sons, 2011.
- [38] H. Toopchi-Nezhad, “Horizontal stiffness solutions for unbonded fiber reinforced elastomeric bearings,” *Struct. Eng. Mech.*, vol. 49, no. 3, pp. 395–410, 2014.
- [39] U. Gerhaher, “Faserverstärkte Elastomerlager – Konzeption und Bemessung,,” BOKU University, 2010.
- [40] U. Gerhaher, A. Strauss, and K. Bergmeister, “Verbesserte Bemessungsrichtlinien für Bewehrte Elastomerlager,” *Bautechnik*, vol. 88, no. 7, pp. 451–458, 2011.
- [41] D. Konstantinidis and J. M. Kelly, “Advances in Low-Cost Seismic Isolation With Rubber,” *Tenth U.S. Natl. Conf. Earthq. Eng. Front. Earthq. Eng.*, 2014.
- [42] M. G. Calabrese A, Spizzuoco M, Serino G, Della Corte G, “Shaking table investigation of a novel, low-cost, base isolation technology using recycled rubber,” *Struct. Control Heal. Monit.*, vol. 22, pp. 107–122, 2015.
- [43] Building Seismic Safety Council (BSSC) of the National Institute of Building Sciences, “FEMA 450 Edition Recommended Provisions For Seismic Regulations For New Buildings And Other Structures P2,” no. Fema 450, 2003.
- [44] F. Naeim and J. M. Kelly, *Design of seismic isolated structures: from theory to practice*. John Wiley & Sons, 1999.
- [45] R. G. Toopchi-Nezhad, H.; Tait, M.J.; Drysdale, “Shake table study on an ordinary low-rise building seismically isolated with SU-FREIs (stable unbonded-fiber reinforced elastomeric isolators),” *Earthq. Eng. Struct. Dyn.*, vol. 38, pp. 1335–1357, 2009.
- [46] M. T. y R. D. H. Toopchi-Nezhad, “Lateral Response Evaluation of Fiber-Reinforced Neoprene Seismic Isolators Utilized in an Unbonded Application 1627-1637, 2008,” *J. Struct. Eng.*, vol. 134, pp. 1627–1637, 2008.
- [47] M. delle I. e dei Trasporti, “Nuove norme tecniche per le costruzioni (NTC): Gazzetta Ufficiale,” 2009.
- [48] M. Araya, “Desarrollo y Fabricación de Aisladores Sísmicos para Edificio Habitacional, Santiago de Chile,” Civil Universidad de Chile, 1994.
- [49] CEN, “European Committee for Standardization. European Standard EN15129,” 2009.
- [50] J. M. Gere and S. P. Timoshenko, “Mecánica de materiales,” *Cengage Learn. México*, 2009.
- [51] J. M. Kelly and D. Konstantinidis, *Mechanics of Rubber Bearings for Seismic and Vibration Isolation*. John Wiley & Sons, Ltd, 2011.
- [52] A. N. Gent, *Engineering with rubber - How to design rubber components*. Munich, Germany: Hanser Publications, 2012.
- [53] L. Mullins, “Softening of Rubber by Deformation,,” *Rubber Chem. Technol.*, vol. 42, pp. 339–362, 1969.
- [54] H. Toopchi-Nezhad, M. J. Tait, and R. G. Drysdale, “Testing and modeling of square carbon fiber-reinforced elastomeric seismic isolators,” *Struct. Control Heal. Monit. Off. J. Int. Assoc. Struct. Control Monit. Eur. Assoc. Control Struct.*, vol. 15, no. 6, pp. 876–900, 2008.
- [55] A. Karimzadeh Naghshineh, U. Akyuz, and A. Caner, “Lateral response comparison of unbonded elastomeric bearings reinforced with carbon fiber mesh and steel,” *Shock Vib.*, vol. 2015, 2015.
- [56] I. M. S. D. L. J. M. P. Thomson., “Development and experimental behavior of HDR seismic isolators for low-rise residential buildings,” *Eng. Struct. J.*, vol. Under revi, 2018.
- [57] H. Toopchi-Nezhad, R. G. Drysdale, and M. J. Tait, “Parametric Study on the Response of Stable Unbonded-Fiber Reinforced Elastomeric Isolators (SU-FREIs),” *J. Compos. Mater.*, vol. 43, no. 15, pp. 1569–1587, 2009.
- [58] G. Russo and M. Pauletta, “Sliding instability of fiber-reinforced elastomeric isolators in unbonded

applications,” *Eng. Struct.*, vol. 48, pp. 70–80, 2013.

ACCEPTED MANUSCRIPT